ISSN 1330-3651 (Print), ISSN 1848-6339 (Online)
https://doi.org/10.17559/TV-20160208145336

COMPARATIVE CFD ANALYSES OF A 2D SUPERSONIC NOZZLE FLOW WITH JET TAB AND JET VANE

Olivera Kostić, Zoran Stefanović, Ivan Kostić

Original scientific paper
In this study, a CFD (Computational Fluid Dynamics) computational model has been established, with the aim to properly simulate complex supersonic flow generated by a 2D convergent-divergent nozzle. For the purpose of rocket engine thrust vector control (TVC) simulations, initially several jet tab positions were used to generate up to 30% shadowing of the nozzle exit, without and with a gap between tab and exit. Numerical results were compared with the existing experimental data, both quantitatively and qualitatively, and fair agreements have been obtained in both senses. The same CFD settings have then been applied for the computational analysis of another TVC type – the jet vane, which was analysed in four different adopted configurations with respect to the nozzle. Stable convergence of solutions has been achieved, up to 40° of vane deflections. Performed calculations have enabled comparisons of the two considered TVC types, in the sense of the achieved thrust force deflections, and thrust losses.

Keywords: *CFD analysis; flow visualization; jet tab; jet vane; supersonic nozzle; thrust vector control*

Usporedna CFD analiza 2D strujanja supersoničnog mlaznika sa spojlerom i s mlaznim krilcem

Izvorni znanstveni članak
U okviru ove studije, ustanovljen je CFD (Computational Fluid Dynamics) proračunski model za potrebe analize kompleksnog nadzvučnog strujnog polja generiranog 2D konvergentno-divergentnim mlaznikom. U cilju simulacije upravljanja vektorom potiska (UVP) raketnih motora, najprije je rabljen spojler, postavljen u nekoliko položaja do maksimalnih 30% zasjenčenja površine izlaznog presjeka, bez procjepa i s procjepom u odnosu na izlaz. Proračunski rezultati uspoređeni su s raspoloživim eksperimentalnim rezultatima kvantitativno i kvalitativno, pri čemu su u oba slučaja dobivena zadovoljavajuća poklapanja. Jednaka CFD podešavanja su zatim uporabljena za kompjutersku analizu još jednog tipa UVP – mlaznog krilca, koje je analizirano u četiri različite usvojene konfiguracije u odnosu na mlaznik. Stabilna konvergencija rješenja je postignuta za sve kutove otklona mlaznih krilaca do 40°. Provedeni proračuni omogućili su usporedbu dva razmatrana tipa UVP, kako u smislu ostvarenog zakretanja sile potiska, tako i u kontekstu gubitaka potiska.

Ključne riječi: *CFD analiza; mlazno krilce; spojler; superonični mlaznik; upravljanje vektorom potiska; vizualizacija strujanja*

1 Introduction

This paper presents several representative cases of an investigation aimed to evaluate the capability of CFD calculations, based on the Reynolds-Averaged Navier-Stokes equations with k-ω Shear-Stress Transport turbulence model, to adequately calculate the flow inside and behind a convergent-divergent nozzle with supersonic Mach number at its exit, including devices positioned in exit domain, aimed for the rocket engine thrust vector control (TVC) simulations. Initially, the flat, wedge shaped obstacles of different heights were positioned at the lower side of nozzle exit section, in order to generate side force that simulates one TVC type, the jet tab. Existing experimental results have been used to derive, establish and calibrate the CFD calculation model for jet tabs, which was then applied for the computational analyses of another TVC type, the jet vanes.

The experimental reference for evaluation of here presented jet tab CFD modeling were two-dimensional (2D) supersonic tests in T-36 wind tunnel in VTI Žarkovo (Military Technical Institute, Belgrade, Serbia), performed by specialist teams from the University of Belgrade, Faculty of Mechanical Engineering and VTI Žarkovo [1]. This investigation was conducted as an experimental research of methods used for thrust vector control of rocket engines. All relevant data presented and used in this paper, which refer to the experimental conditions, geometries and qualitative and quantitative results, have been adopted from [1-4]. Test fluid was air, and tests were performed using a vast number of different tab shapes, sizes, positions and gaps between the tab and exit section. Experimental facility with tab at the nozzle exit is shown in Fig. 1.

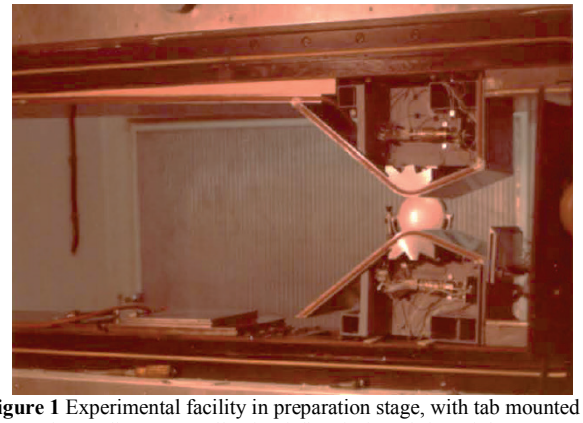

Figure 1 Experimental facility in preparation stage, with tab mounted at lower divergent wall exit; airflow is from left to right [1]

First part of this paper is confined to the 2D computational analysis of a simulated jet tab, adjustable in its vertical position and gap. Calculations have been made for tab heights generating 10%, 20% and 30% shadowing of the exit section area, and they were analyzed without a gap between tab and the exit, and with 1.74 mm gap, which corresponds to 1.2% of the exit section height. Computational and meshing algorithms have been established, and numerical results have been qualitatively and quantitatively compared and verified with experiments. Those CFD settings have then been applied for the computational analyses of four adopted jet vane types, that were not tested during the experiments reported in [1]. The chord and maximum deflection angle

of vanes have been set in a way to generate aproximately the same maximum effective exit shadowing of about 30%, applied in this paper within jet tab analyses.

Established computational model has proven its robustness and capability to obtain stable and full convergence for all analyzed cases, and provide valuable data for comparative 2D analyses of different TVC types.

2 TVC using jet tabs and jet vanes – basic theory

Some of the commonly used types of TVC, as well as the order of values of thrust vector deflection angles achieved by them, are shown in Fig. 2.

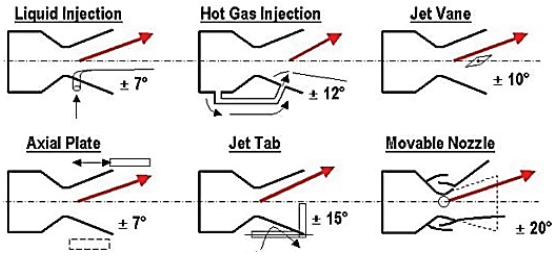

Figure 2 Some common types of TVC [5]

The jet tab system consists of spoilers mounted at the nozzle exit which, when inserted locally in the outcoming gas flow, generate the required side control force F_Y. The examples of possible jet tab arrangements are shown in Fig. 3.

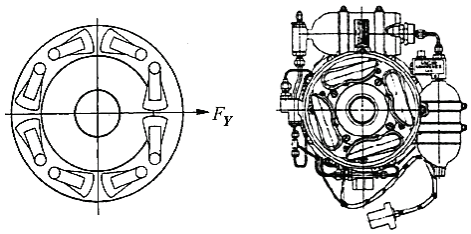

Figure 3 The jet tab control systems [6, 7]

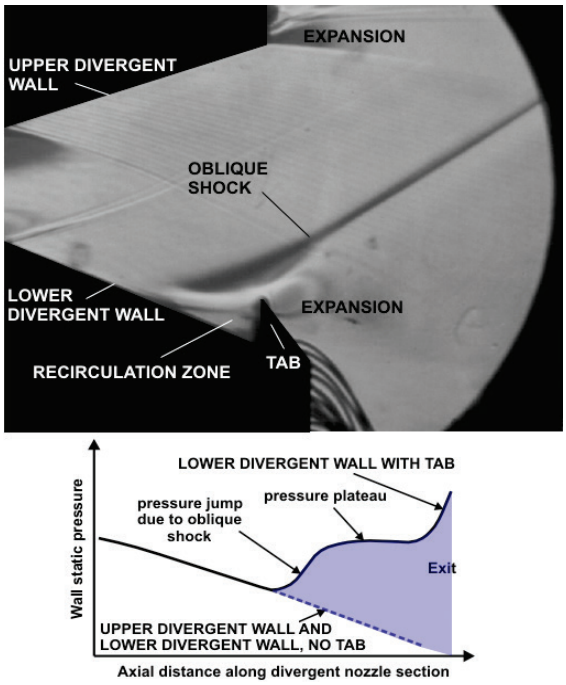

Figure 4 Schematics explaining general tab influence on the flow pattern inside the 2D nozzle, and the wall pressure distributions

The tab control systems [6] provide rather simple and compact TVC design, low required actuator power, reasonably small vector control losses, etc. On the other hand, the flow field patterns in actual three-dimensional (3D) nozzles with circular cross sections, with tabs actuated, are very complex. Because of that, the initial analyses are usually performed on simplified two-dimensional models. Such 2D experiments (as in Fig. 1) are usually conducted in supersonic wind tunnels, using air as working fluid, and they are called the "cold" tests.

The general influence of a tab on supersonic flow in divergent section of a 2D nozzle is schematically shown in Fig. 4. The protruding tab produces a recirculation zone (separated boundary layer domain) in front of it, which acts as a "fluid wedge" and generates an oblique shock wave. Behind it, the pressure on the lower divergent wall increases with respect to the distribution that would correspond to the case without tab. This difference in pressures between the lower and upper divergent walls (shaded area on pressure diagram in Fig. 4) generates side force F_Y, used for thrust vectoring. Pressure jump on the lower wall starts at the upstream end of the recirculation zone, and it is followed by the "pressure plateau" domain. Evaluation of pressure distribution in this domain is the most important part in these investigations.

Unlike tabs, the basic principle of TVC generated by jet vanes is simpler – they are actually small wings positioned in the supersonic nozzle flow, whose change in deflection angle (i.e. angle of attack) produces the primary control force. They represent the oldest TVC concept, applied on the first ballistic missile - the V-2, by the end of the World War II (Fig. 5).

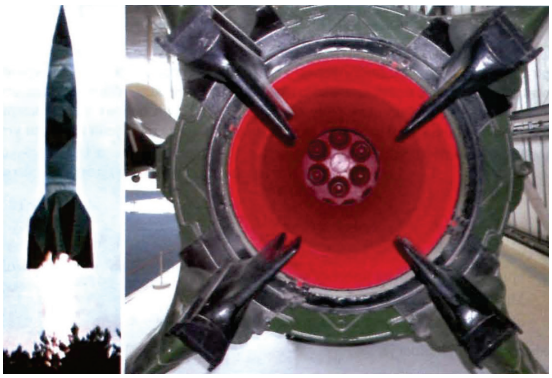

Figure 5 Jet vanes applied on the V-2 missile [7], positioned behind the nozzle exit

Jet vanes are also very widely used on the modern rocket propulsion systems, in a variety of design arrangements, and can generally be classified as internal (positioned inside the nozzle, or in a shroud as nozzle extension), or external (in free flow at nozzle exit or behind it). Selection of the concept depends on the actual control and design requirements. A general drawback of the vanes is a certain loss of nozzle thrust at their zero deflection, due to the vane's profile drag; their advantage over the tabs is the capability to generate both the rolling moment of the missile and the thrust deflection, while tabs can only alter the thrust force deflection angle. Similarly as tabs, the vane design concepts can initially be analysed as simplified 2D models, determining their primary advantages or drawbacks.

3 General description of the experiments

All experiments used as reference in this paper, involving jet tab analyses, were performed in T-36 indraft supersonic wind tunnel, at VTI Žarkovo, on a scaled convergent-divergent nozzle model with rectangular cross section. The actual geometry [1, 3] of the nozzle has been used to define the control volume for CFD calculations, for nominal exit Mach number M = 2.6 (Fig. 6). The width of the wind tunnel test section (distance between the side walls) was 249 mm. Such experiments are qualified as 2D flow tests.

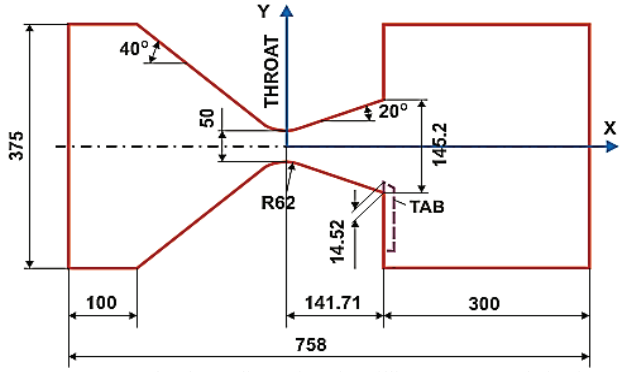

Figure 6 Control volume dimensions in millimetres; example is given for 10% exit shadowing, without gap

The initial pressure in vacuum tank was 5 mbar for all blows (test runs). On the other hand, the inlet values varied to a certain extent, depending on ambient conditions during each blow. These values were applied in CFD calculations for the definition of inlet and outlet parameters. For example, in case of 10% shadowing tab without gap [1], ambient pressure was 1018.313 mbar, temperature 286.75 K, and they influenced other parameters, such as the reference Mach number in front of the nozzle M = 0.086, total pressure in test section of 1010.542 mbar, etc. (more details can also be found in [8]). Pressures were measured in the rear domains of the divergent walls and tabs using three "Scanivalve" type S instruments, with automated data acquisition to a customized computer system. Pressure measurements represent quantitative data records. The flow pattern records were obtained by Schlieren photos taken for each test run, and they were used for qualitative assessments of here presented CFD calculations of jet tabs.

4 Description of the applied calculation procedure

All results presented in this paper have been obtained by 2D compressible flow modelling in ANSYS Fluent 14, using control volume shown in Fig. 6, and adding the appropriate TVC geometry.

Calculations of flow characteristics were performed using RANS (Reynolds-Averaged Navier-Stokes) equations combined with k-ω SST (Shear-Stress Transport) turbulence model [9-11]. The most important settings that have been established are:

- Solver: 2D density-based.
- Model: viscous, k-ω SST (two-equation) with compressibility effects and curvature correction.
- Fluid: air, ideal gas, viscosity by Sutherland law, three coefficient method.
- Boundary conditions: control volume inlet and outlet parameters as defined in [1] for the given test case.
- Calculation: flow type – supersonic, FMG - the Full Multi-Grid solution initialization at 4 levels [11, 12], initial optimum reordering of the mesh domain using Reverse Cuthill-McKee method [12], active solution steering, applying Courant number optimization for the achieved solution convergence stage (maximum set to 10, although in some phases drastic "manual" reductions had to be applied), etc. With options "flow parameters", "turbulent kinetic energy" and "specific dissipation rate" set to "first order upwind", stable convergence considering mass flow rate and scaled residuals has been achieved after 5000 ÷ 16000 iterations, depending on the flow and geometry complexity of the analysed case.

Those settings have been very carefully established, after a substantially long series of test runs, by the authors of this paper, during the initial investigations of nozzle flow with free exit, and nozzle with 10% shadowing tab without gap [8], and they have proven their value in here presented analyses as well.

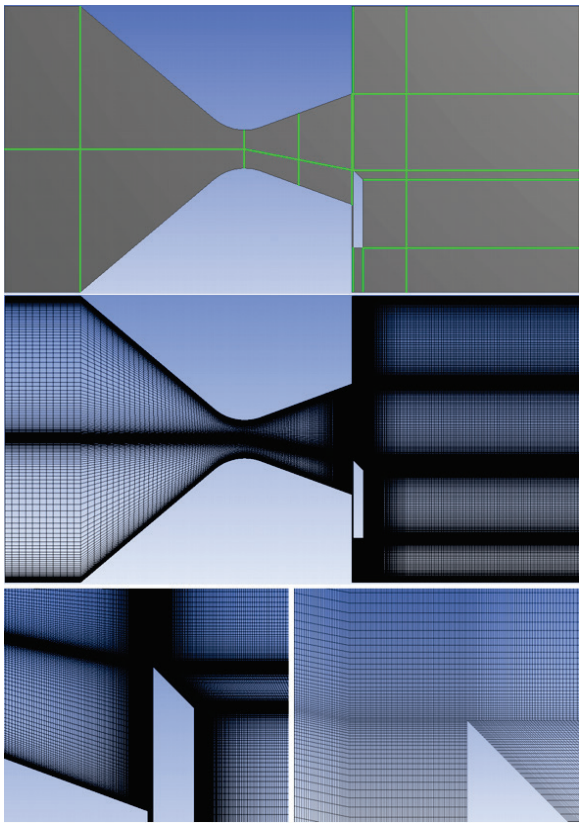

Figure 7 Control volume segmenting, and mesh for 30% shadowing and 1.2% gap, with 388000 elements; details are showing the tab top

For all tab cases, structured meshes were generated, using mapped face meshing option (example is shown in Fig. 7, for the most complex of the considered tab cases). Attention was paid to proper control volume segmenting and edge sizing. Static mesh adaptation has been made using different bias types and factors, in order to progressively increase the number of elements in critical flow domains such as walls, sharp corners, gaps and tab edges. This approach has given better results, than the Fluent's automatic adaptation option. A further

improvement has recently been made, with respect to previous analyses [8], by fine adjusting bias factors so that mesh cells are practically of the same sizes at the control volume segment junctions, giving very smooth transition from one mesh domain to another (see Fig. 7, bottom-right). This has provided better solution convergences, higher quality of flow field visualisations, and also improvements in plateau pressure distributions, compared to previous work.

The number of mesh elements is ranging from approximately 200000 for 10% shadowing, up to about 400000 elements for 30% shadowing cases (experiments to increase it further to 700000 elements brought no relevant benefits to the results). Satisfactory mesh quality has been achieved, which all-together enabled time and resource efficient calculations, although the here applied turbulent model is very robust itself, and has rather low sensitivity to mesh properties and sizing.

5 CFD analysis of jet tabs and comparisons with the experimental results

All CFD calculations presented in this paper have been performed with nozzle geometry, and the inlet and outlet parameters adopted from the actual experimental setups [1], which correspond to the nozzle exit Mach number M = 2.6. Detailed initial verifications of the computational model and results, with respect to the experiments, have been performed for the free nozzle exit case (including exit Mach number, wall pressures, etc.), and 10% shadowing tab without gap, and they have been published by the authors of this paper in [8]. (Also, very interesting CFD analyses, using higher order turbulence models than in this paper, considering the same experiments [1], but with exit Mach number M = 2.3 and 10% shadowing tab, can be found in Živković at al. [13].)

Further analyses have been spread to shadowing ratios 10%, 20% and 30% without gap, and with 1.2% gap – cases adopted from [1]. Ratios beyond 30% can hardly be achieved in operational practice with 3D nozzles (practical limit in [14] is set to about 20%), except in case of small rocket nozzles (40% value, mentioned in [7]). In case of rocket engines, zero gap would represent an "ideal" tab, with maximum effectiveness; small gap is allowable for different technological and/or operational reasons. Larger gaps, of the order of 5% ÷ 10%, would substantially degrade tab efficiency [3], [14], etc.

Due to the limited length of paper, two cases will be presented in details. The first one is the 10% shadowing tab (with and without gap), for which relatively quick convergences have been achieved; the second is 30% shadowing, which, on the other hand, has been quite challenging both for the computational model and the hardware resources.

For qualitative assessments and comparisons with the experiments, the calculated velocity contours (obtained directly in Fluent), and density gradients (post-processed in CFD Post) have been selected, because they quite clearly depict the oblique shocks, recirculation zones and flow expansion domains. They are compared with the appropriate Schlieren photos, published in [1], in Figs. 8 ÷ 11 (unfortunately, small 1.2% gaps have not been captured on photos from the experiments).

The visual inspections indicate that performed CFD calculations, with the applied settings and meshing, have properly depicted all characteristic flow field domains, compared with Schlieren photos from the experiments.

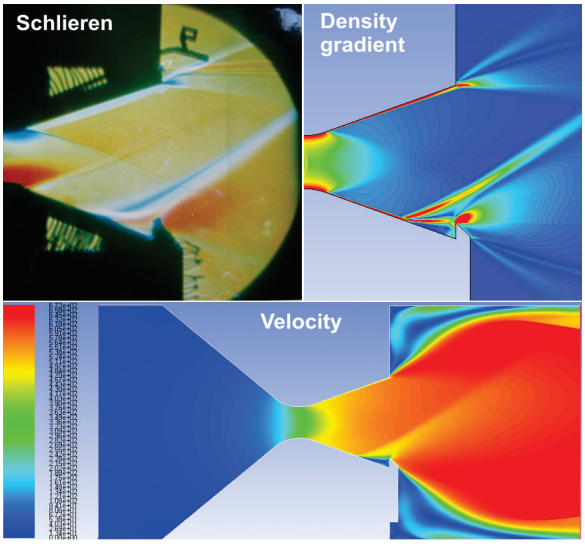

Figure 8 Flow visualisations for 10% shadowing tab, no gap

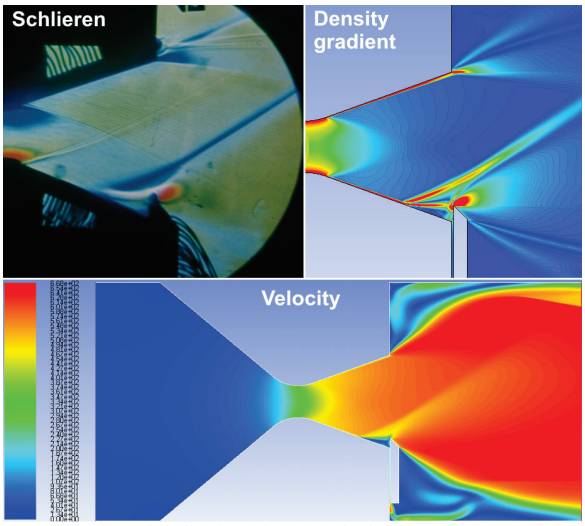

Figure 9 Flow visualisations for 10% shadowing tab and 1.2% gap

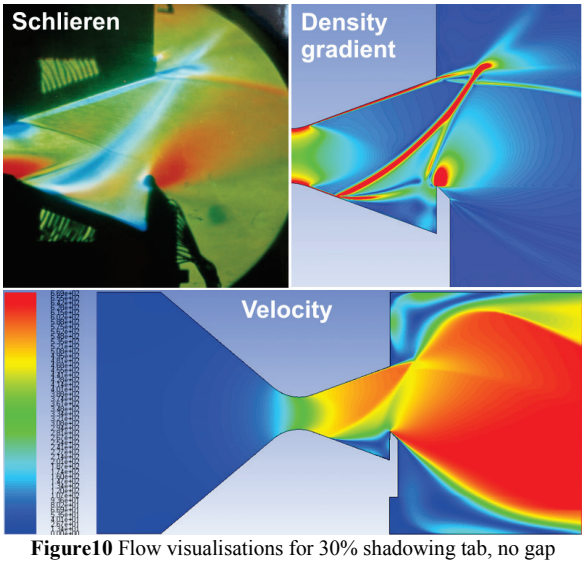

Figure10 Flow visualisations for 30% shadowing tab, no gap

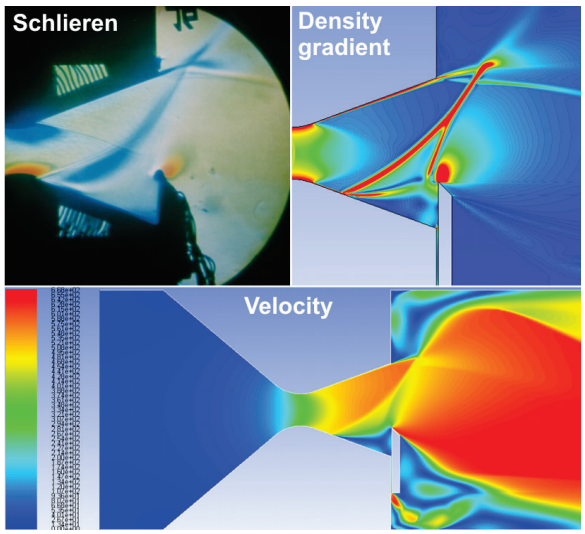

Figure 11 Flow visualisations for 30% shadowing tab and 1.2% gap

For 10% and 30% shadowing tabs with gap, the oblique shock is slightly closer to the nozzle exit (both in calculation and the experiment), due to the outflow through the gap, compared to the cases without gap. Oblique shock angles and positions are properly determined, while recirculation zones (i.e. subsonic fluid wedges, which trigger shock waves) are well defined too. Also, the expansion zones show good spatial agreements with experimental photos. It should be noted that the density gradients, visualized by CFD Post, are shown as absolute values - same colour types define compression and expansion, while Schlieren, at the time of the experiments, was "inverting" colours in vertical direction of the photos. Thus, the compatibility in colours between photos and CFD density gradient images was impossible to achieve (although variation in colours in Schlieren photos is basically generated by flow field density gradients). Obtained velocity contours also give very good insight in flow patterns within the entire control volume, including domains not covered by experimental photos, such as flow inside and behind the gap, etc.

Quantitative assessments have been focussed on evaluation of static pressure differences obtained on the upper and lower divergent nozzle walls, generated by different exit shadowings. As mentioned in Chapter 2, this pressure difference generates the side component of the thrust force (the control force – see also Fig. 4).

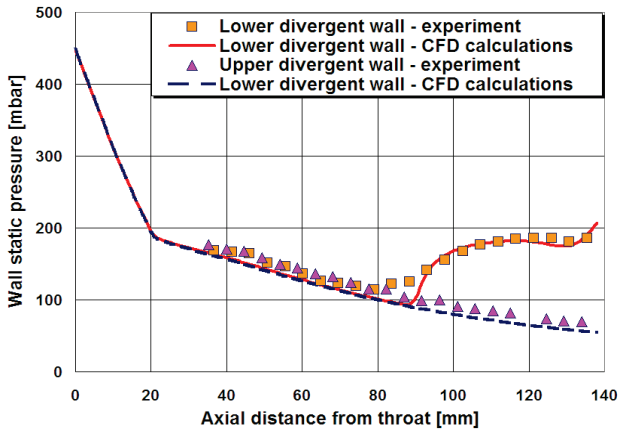

Figure 12 Comparison between the experimental and calculated pressure distributions, 10% shadowing, no gap

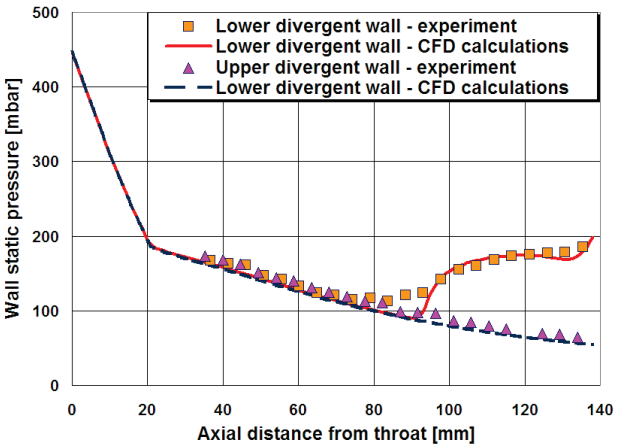

Figure 13 Comparison between the experimental and calculated pressure distributions, 10% shadowing with 1.2% gap

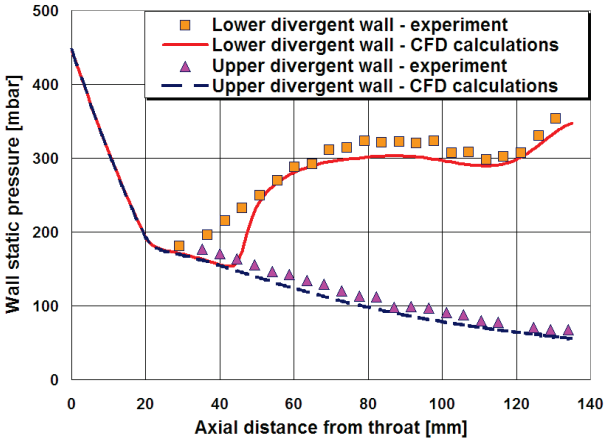

Figure 14 Comparison between the experimental and calculated pressure distributions, 30% shadowing, no gap

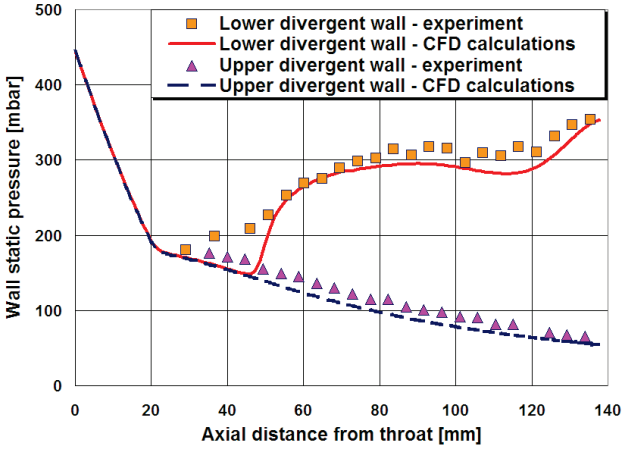

Figure 15 Comparison between the experimental and calculated pressure distributions, 30% shadowing with 1.2% gap

Considering both analysed 10% shadowing cases, from the engineering point of view, calculated differences between pressure plateau values on lower walls, and undisturbed flow pressures on upper walls, compared with the experiment, are very good (Figs. 12 and 13). Keeping in mind that this level of flow complexity presented no problems for the established calculation model, such results are expected.

The two 30% shadowing cases required much more iteration steps, manual reduction and control of Courant number, etc., but the final outcome is proper numerical convergence of both cases. It can be noticed that the

calculated pressures on upper and lower walls are slightly shifted below the experimental values (and this trend is also reported in [3], where another calculation method has been applied). On the other hand, since the control force is generated by pressure difference, agreements between calculated and experimental pressure differences in Figs. 14 and 15 can be treated as fair for practical engineering calculations (keeping in mind the flow field complexity generated by such amount of shadowing).

It should also be noticed that pressure jumps on lower walls where oblique shocks are generated, obtained by the calculations, are more abrupt than those obtained in experiments. An obvious explanation might be that here presented calculations have been performed with smooth walls, while wind tunnel walls had orifices for pressure measurements, which inherently induced certain disturbances in boundary layer domain, and caused its earlier interaction with the shock wave, and thus earlier pressure increase towards the pressure plateau domain (such orifices would not exist on rocket nozzle walls).

All previous general conclusions apply for 20% shadowing cases as well. Values obtained for this tab setting (with and without gap) have been included in the analyses presented in Chapter 7.

6 CFD analysis of jet vanes

After establishing the overall computational model and mesh settings on jet tab cases, the same CFD settings for nozzle calculations have been used as "virtual wind tunnel" for the analyses of another type of TVC devices, the jet vanes (which, as already mentioned, were not tested at the time when experiments reported in [1] were performed). As for the tab, the nominal Mach number is M = 2.6 at nozzle exit.

For present 2D analyses, a jet vane with symmetrical double-wedge airfoil has been selected. Thickness ratio of 10% has been adopted, with chord length of 70 mm. The maximum deflection angle has been selected to be δ = 40°, which, with the applied chord length, generates about 31% of equivalent exit shadowing. This is practically the same order of maximum exit shadowing (30%) generated by tabs, that have been analysed in this paper.

The four different jet vane-nozzle configurations have been numerically analysed, with rotation axis at the mid-chord position. Examples of meshes applied for them, for zero vane deflection, are shown in Fig. 16, and they have been generated using the same general principles as applied for the jet tabs. For other vane deflection angles, they were modified by keeping the same number of elements in characteristic mesh zones, but optimizing mesh bias factors according to the given vane position.

Internal jet vane, denoted as V1 in Fig. 16, is placed inside the divergent nozzle domain, with trailing edge at nozzle exit, when not deflected. Jet vane V2 is placed with the rotation axis at the nozzle exit, while external vane V3 is placed outside the nozzle, with its leading edge on nozzle exit, in undeflected position. Vane V4 is also an internal vane case (as vane V1), but placed within a shroud, attached to the nozzle exit.

Initial calculations have been performed for zero deflection angle δ = 0°. Obtained velocity contours are shown in Fig. 17. Although the vanes are not deflected in this case, the total thrust of the empty nozzle is reduced as a consequence of the form drag of the vane (wakes behind the vanes are visible in Fig. 17). This is not the case with jet tabs which, when "undeflected", do not spoil the nozzle flow.

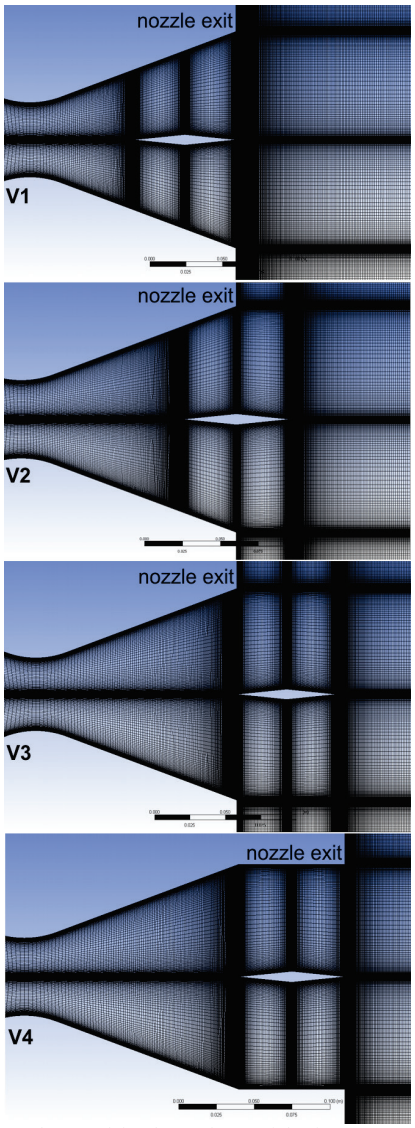

Figure 16 Meshes used for the analyses of the four types of jet vanes; examples are shown for vanes at zero deflection angle

The other analyzed vane deflections, all in nose down direction, were δ = 15°, 30° and 40°. Later on, for more appropriate presentation of diagrams, deflection δ = 25° had to be additionally calculated for vanes V1 and V4.

The primary normal or side force, i.e. the control force, is generated by the vane, and it depends on its deflection angle. In cases when shock waves generated on its leading edge do not collide with the nozzle walls, the control force is produced by the vane itself. In this case, the static pressure distributions on the upper and lower divergent walls are the same, producing equal, but opposed normal force components, which cancel each other. On the other hand, in case of nose-down vane deflections, when shock formed on the leading edge collides and reflects from the upper divergent wall, pressure on this wall behind the shock increases, generating additional side force which opposes the vane-

generated normal force, thus decreasing the overall control effectiveness.

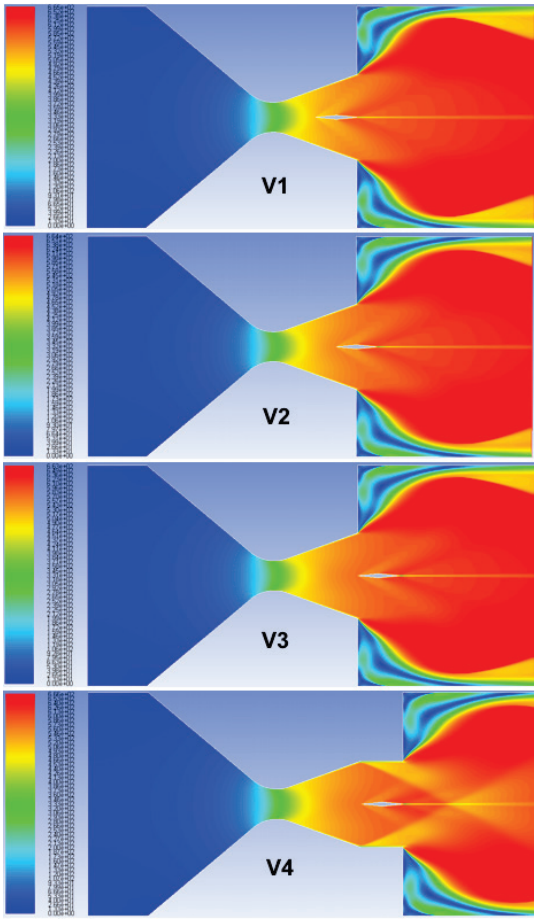

Figure 17 Velocity contours for jet vanes at deflection angle $\delta = 0°$

Also, when a detached bow wave is generated in front of the vane, it may collide both with the upper and the lower nozzle walls. In this case, the upper wall domain behind the shock generates opposing, while lower wall domain generates contributing control force, with respect to the basic normal force on the vane. Thus, the total control force is the sum of all these components, and it depends on the selected vane size, deflection angle, and the applied nozzle-vane configuration. All mentioned cases can be clearly depicted in Figs. 17 ÷ 20.

When the vane deflection is $\delta = 0°$, the flow field is symmetrical in its upper and lower half domains, generating zero resultant side force. At the deflection of $\delta = 15°$, all oblique shocks are attached to the vane leading edge, and do not collide with the nozzle (or shroud) walls. The exception is vane V1, where shock wave touches the very end of the upper nozzle wall, so a reasonably small negative influence on total side force can be expected due to this effect.

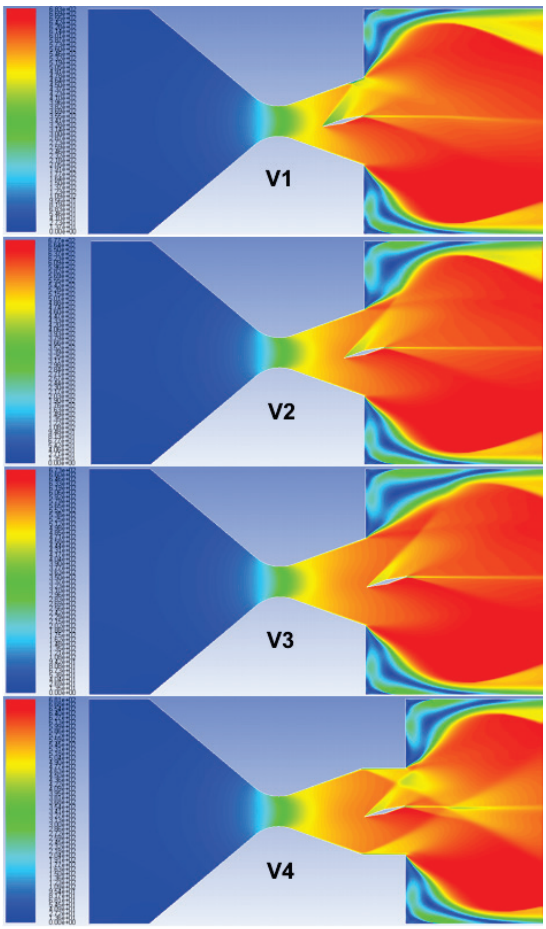

Figure 18 Velocity contours for jet vanes at deflection angle $\delta = 15°$

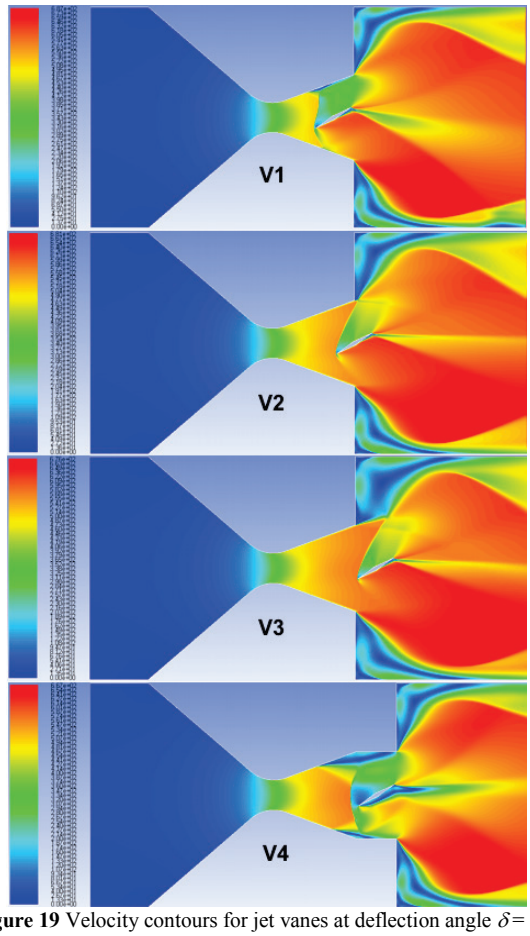

Figure 19 Velocity contours for jet vanes at deflection angle $\delta = 30°$

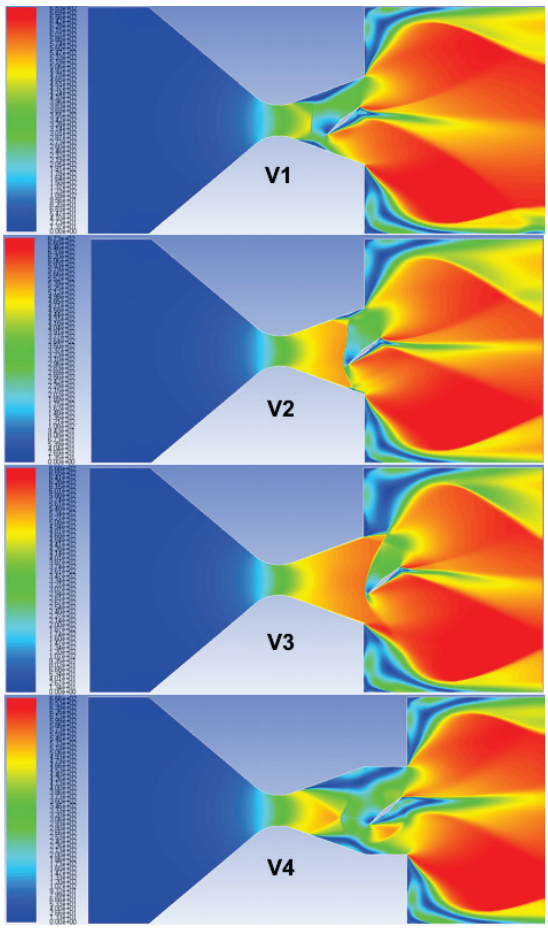

Figure 20 Velocity contours for jet vanes at deflection angle $\delta = 40°$

At the deflection of $\delta = 30°$, the detached bow shocks are generated on the leading edges of the vanes. In cases of V2 and V3, they do not interfere with nozzle walls, preserving the effectiveness of these two types. Opposite to that, the bow shocks on V1 and V4 strongly interfere with the upper and lower nozzle (shroud) walls, where the influence on upper walls is obviously more significant, generating unfavourable influence on the control force. Finally, at the deflection of $\delta = 40°$, only bow shock on vane V3 does not collide with the nozzle, while in case of vane V2 it influences pressures on both upper and lower nozzle walls. On the other hand, bow waves on V1 and V4 are strongly detached, and generate extremely complex flow field patterns inside the nozzles.

7 Discussion of the numerical results

In order to make quantitative comparisons between the two analysed TVC devices, the jet tabs and jet vanes of the adopted geometries, calculations of the normal and axial force components had to be performed.

For a conical nozzle with free exit, the axial thrust force [15] can be obtained from the Eq. (1):

$$F_0 = \dot{m}_e V_e + (p_e - p_0) A_e, \tag{1}$$

where $\dot{m}_e$ is the mass flow rate, V_e is the exit velocity of the propulsive flow perpendicular to exit area A_e, p_e is the static pressure at exit and p_0 represents is the static ambient pressure, surrounding the nozzle. In case of rocket propulsion systems, F_0 is also equal to the sum of axial forces acting on the internal nozzle and the combustion chamber walls. On the other hand, for nozzle flow simulated in wind tunnel (real or virtual), F_0 can formally be written as:

$$F_0 = -\dot{m}_t V_t - (p_t - p_0) A_t + F_{DUX} + F_{DLX}, \tag{2}$$

In this case, it has been assumed that only isolated divergent nozzle domain exits, from the throat to the exit; first two members in (2) represent the influence of the installation in front of the throat (values in throat, denoted by subscript t), while F_{DUX} and F_{DLX} are axial force components acting on the upper and lower divergent nozzle walls. Calculations performed in Fluent, using its capabilities to compute the mass flow rate, the integrals of velocity and pressure over assigned areas, as well as the forces and their components on the walls, gave very good agreements between Eqs. (1) and (2), for tested free exit case. This is of primary importance for thrust force calculations with an obstacle (tab or vane) at exit, because proper application of Eq. (1) in such cases may become complicated.

Using previous principle, for axial force component calculations, the following equation has been applied:

$$F_X = -\dot{m}_t V_t - (p_t - p_0) A_t + F_{DUX} + F_{DLX} + F_{OX}, \tag{3}$$

The last member F_{OX} (subscript O stands for obstacle) represents axial force component acting on a jet vane, or the jet tab in its domain exposed to the exit flow. For the normal force, the following equation has been used:

$$F_Y = F_{DUY} + F_{DLY} + F_{OY}, \tag{4}$$

Attention should be paid to the proper application of signs for all members in Eqs. (3) and (4).

Obtained axial and normal components of the thrust force for different tab shadowing ratios and vane deflections, are customary presented as relative values, compared to the free exit thrust force F_0. They are denoted as F_X/F_0 and F_Y/F_0. The total thrust force deflection is calculated as:

$$\varphi = \operatorname{atan}(F_Y / F_X), \tag{5}$$

Fig. 21 shows the computed values of relative force components for the jet tab without gap, and with 1.2% gap, and for the four analysed jet vane configurations, versus the generated thrust force deflection angles. Maximum deflections of the order of 16° ÷ 17° have been achieved by jet tabs, corresponding to 30% exit shadowing (see also Fig. 2). Slightly smaller values, 14° ÷ 16° have been obtained for external jet vanes V3 and V2 respectively, at $\delta = 40°$ deflection angles, or about 31% of equivalent exit shadowing. Larger maximum thrust deflection was obtained by vane V2, whose front half is positioned inside the nozzle and thus at lower supersonic Mach number values than V3, with its nose at exit. This gave V2 slightly higher effectiveness because, in

supersonic flow, the lift curve slope decreases with Mach number increase, and vice versa. Internal vanes V1 and V4 have achieved the lowest thrust force deflections, of about 9° ÷ 10° (also see Fig. 2), for the same vane maximum deflections of δ = 40°, which is the consequence of very complex bow wave interference with nozzle walls, and loss of effectiveness due to that.

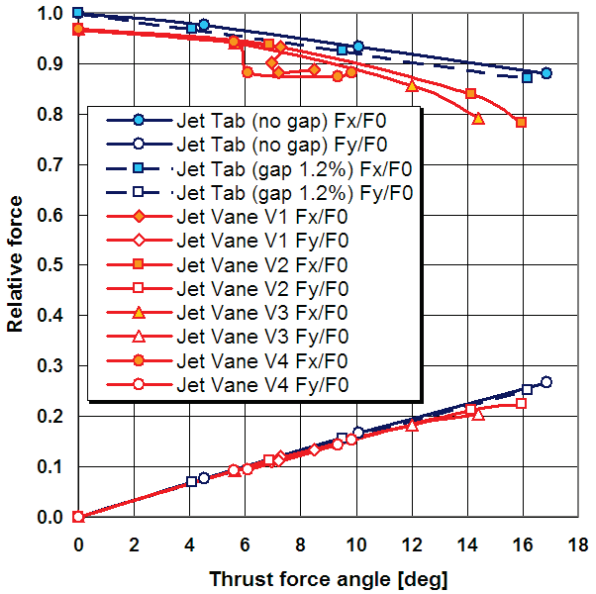

Figure 21 Relative axial and normal forces for achieved resultant thrust deflection angle

Relative axial force losses (differences between F_X/F_0 and the ideal value of 1) are larger in case of all analyzed vanes, compared to the jet tabs. On the other hand, the slopes of relative side forces F_Y/F_0 with respect to the thrust force deflection are practically the same for all cases.

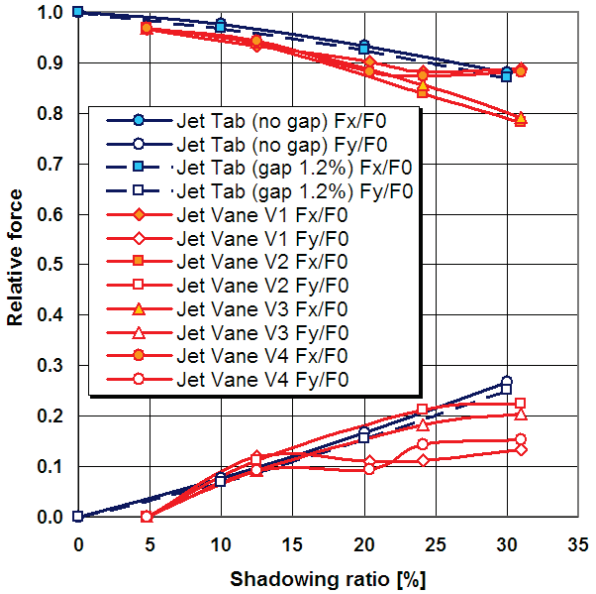

Figure 22 Relative axial and normal forces for the corresponding effective exit shadowing ratios

Very important information can also be obtained from Fig. 22, where relative thrust force components are presented with respect to the effective exit shadowing, proportional to the vane angular deflections. While jet tabs, as well as vanes V2 and V3, show quite stable and progressive trend of change, curve slopes for vanes V1 and V4 become non-uniform for effective shadowing beyond 12.5%, which would certainly present problems in thrust vector automatic control programming.

Another issue considering vanes is the fact that they are permanently exposed to the exhaust flow, including cases when they are not deflected. Due to that, relatively large airfoil thickness ratio of 10% has been selected for here presented analyses (empirically adopted), because in "real life" conditions, vanes are exposed to extremely hot gas flow and collisions with small solid propellant particles, and such thickness ratio is necessary in order to preserve their structural integrity. Due to that, when here analysed vanes are undeflected, they generate almost 5% of exit shadowing (Fig. 22), and some 3% loss in axial force (Fig. 21), which is not the case with jet tabs. On the other hand, in actual 3D applications on missiles (where, most often, four vanes are symmetrically distributed on nozzle circumference), using proper combination of deflections, vanes can produce both angular thrust deflection and rolling moment, while tabs in 3D applications can generate only thrust force vectoring. Unfortunately, this advantage of jet vanes over tabs cannot be simulated within the 2D analyses.

It is quite clear that alternations in here applied jet vane chord, thickness ratio, airfoil type, disposition with respect to the nozzle, etc. would alter the obtained values to a certain extent. On the other hand, the primary aim of this paper has been to verify the capability of the established calculation algorithm, calibrated with respect to the existing experimental results, to efficiently deal with other TVC cases, and to be used for comparison and optimizing purposes in the initial design stages, within 2D analyses.

8 Conclusion

In this paper, a computational model for two-dimensional TVC analyses has been established, and calculations have initially been performed for several jet tabs cases, with maximum shadowing of 30% of nozzle exit. For the calibration of the applied computational options and meshing techniques, experimental data have been used, and qualitative and quantitative comparisons have been made. After fair agreements have been achieved with respect to experiments, the same general settings have been used for the analyses of four adopted jet vane types, up to the angular deflections that generate approximately the same maximum effective exit shadowing. The numerical solutions for all vane types analysed in this paper have shown stable convergence, in spite of extremely high complexity of the flow field in most cases. This has confirmed the ability of the applied computational and mesh settings, established during jet tab analyses, for successful comparative 2D analyses of other similar TVC devices.

9 References

[1] Jojić, B.; Stefanović, Z.; Blagojević, Đ.; Vučković, S.; Rajčić, Z. Research in Modern Rocket Propulsion TVC (in

Serbian). University of Belgrade, Faculty of Mechanical Engineering and VTI Žarkovo, Belgrade, Serbia, 1984.
[2] Jojić, B.; Milinović, M.; Stefanović, Z.; Blagojević, Đ. Pressure Distribution in Rocket Nozzle with Mechanical System for TVC. // AIAA Paper 87-1824, USA, 1987.
[3] Stefanović, Z. Research of Fluid Flow and Pressure Distribution in Supersonic Nozzle in Connection with the Vector Thrust Control (in Serbian). // Doctoral thesis, University of Belgrade, Belgrade, Serbia, 1986.
[4] Stefanović, Z.; Miloš, M.; Todić, I.; Pavlović, M. Investigation of the Pressure Distribution in a 2D Rocket Nozzle with a Mechanical System for Thrust Vector Control (TVC). // Strojarstvo. 53, 4(2011), pp. 287-292.
[5] Scott, J. A. Missile Control Systems, Aerospaceweb.org. 2004. http://www.aerospaceweb.org/question/weapons/q0158.shtml (24.06.2015).
[6] Hollstein, H. J. Jet Tab Thrust Vector Control. // J. Spacecraft. 2, 6(1965), pp. 927-930. https://doi.org/10.2514/3.28316
[7] Živković, S. Technical Solutions and Gasdynamic Efficiency of Thrust Vector Control Systems for Rocket Missiles (in Serbian). Military-Technical Institute, Belgrade, Serbia, 2015.
[8] Kostić. O.; Stefanović, Z.; Kostić. I. CFD Modeling of Supersonic Airflow Generated by 2D Nozzle with and Without an Obstacle at Exit Section. // FME Transactions. 43, 2(2015), pp. 107-113. https://doi.org/10.5937/fmet1502107k
[9] Wilcox, D. C. Turbulence Modeling for CFD, DCW Industries, Inc., California, USA, 2006.
[10] ANSYS FLUENT 14.0: Theory Guide, ANSYS, Inc., Canonsburg, PA, USA (2011).
[11] ANSYS FLUENT 14.0: User's Guide, ANSYS, Inc., Canonsburg, PA, USA (2011).
[12] ANSYS FLUENT 14.0: Tutorial Guide, ANSYS, Inc., Canonsburg, PA, USA (2011).
[13] Živković, S.; Milinović, M.; Adamec, N. Experimental and Numerical Research of a Supersonic Planar Thrust Vectoring Nozzle via Mechanical Tabs. // FME Transactions. 42, 2(2014), pp. 205-211. https://doi.org/10.5937/fmet1403205z
[14] Davidović, N.; Miloš, P.; Jojić, B.; Miloš, M. Contribution to Research of Spoiler and Dome Deflector TVC Systems in Rocket Propulsion. // Technical Gazette. 22, 4(2015), pp. 907-915. https://doi.org/10.17559/TV-20140621063849
[15] Elements of Aircraft and Missile Propulsion // Engineering Design Handbook / U.S. Army Missile Command. Redstone Arsenal, AL, 1969.

Authors' addresses

mr. sc. Olivera Kostić, dr. sc. candidate, Teaching Assistant
University of Belgrade
Faculty of Mechanical Engineering
Kraljice Marije 16, 11000 Belgrade, Serbia

dr. sc. Zoran Stefanović, Full Professor
University of Belgrade
Faculty of Mechanical Engineering
Kraljice Marije 16, 11000 Belgrade, Serbia

dr. sc. Ivan Kostić, Full Professor
University of Belgrade
Faculty of Mechanical Engineering
Kraljice Marije 16, 11000 Belgrade, Serbia
E-mail: ikostic@mas.bg.ac.rs